Journal of Pharmaceutical and Biomedical Analysis 50 (2009) 475–490

Contents lists available at ScienceDirect

Journal of Pharmaceutical and Biomedical Analysis

journal homepage: www.elsevier.com/locate/jpba

In vitro and *in vivo* investigation of metabolic fate of rifampicin using an optimized sample preparation approach and modern tools of liquid chromatography–mass spectrometry

Bhagwat Prasad, Saranjit Singh*

Department of Pharmaceutical Analysis, National Institute of Pharmaceutical Education and Research (NIPER), Sector 67, S.A.S. Nagar 160 062, Punjab, India

ARTICLE INFO

Article history:
Received 6 March 2009
Received in revised form 13 May 2009
Accepted 14 May 2009
Available online 22 May 2009

Keywords:
Rifampicin
Metabolite enrichment
Metabolite identification
Characterization
LC–MS
HR-MS

ABSTRACT

Biotransformation products of rifampicin formed *in vitro* and *in vivo* were identified using modern tools of liquid chromatography–mass spectrometry (LC–MS). For the same, first the mass fragmentation pattern of rifampicin was delineated by conducting multiple-stage MS (MS^n), high resolution MS (HR-MS) and hydrogen/deuterium exchange MS (HDE-MS) experiments in an electro-spray ionization (ESI) mode. Then *in vitro* metabolism was investigated by incubating the drug with rat liver S9 fraction and microsomes at pH 7.4 in the presence of NADPH for 2 h at 37 °C. *In vivo* metabolites were generated by administering the drug to Sprague–Dawley (SD) rats ($n = 5$) at a dose of 50 mg kg^{-1} and collecting blood, urine and feaces at different time points up to 72 h. The samples were processed using an optimized sample preparation approach, involving protein-precipitation using acetonitrile; followed by liquid-freeze separation at −20 °C; and solid-phase extraction of aqueous layer. HPLC conditions were optimized using known standards of rifampicin metabolites or degradants. The extracted and concentrated samples were then subjected to LC-DAD–MS/time-of-flight (LC-DAD–MS/TOF) analyses in both ESI positive and negative modes. The structures of metabolites were elucidated by comparing their accurate mass values and fragmentation patterns with those of rifampicin, use of *in silico* identification tools and relative retention time matching with the standards. The nature of the metabolites and their relative amounts varied. In total, 21 metabolites were identified, of which many structures were new, not reported till date.

1. Introduction

In modern practice of drug discovery and development, comprehensive investigation of drug metabolism is necessary to optimize lead compounds, and to explain mode of their efficacy, clearance, inter-individual variation and toxicity. Drug metabolism studies include metabolic stability, cytochrome P450 (CYP) induction/inhibition potentials, reaction phenotyping and metabolite identification. These are generally carried out by employing *in vitro* systems, followed by *in vivo* studies on rodents and humans. Compared with drug metabolism science of four decades ago, there are paramount improvements, primarily catalysed by the availability of *in vitro* tools for metabolite generation, and use of advanced analytical modalities, like liquid chromatography–mass spectrometry (LC–MS) [1–6]. The modern MS tools help to identify the biotransformation products even without the need for separation of individual metabolites or in some cases sample processing (*e.g.*, urine and bile can be analyzed directly). In fact, MS has been utilized in various modes, like multiple-stage MS (MS^n), high-resolution MS (HR-MS) and hydrogen/deuterium exchange MS (HDE-MS) for the elucidation of unknown structures, including metabolites [7–11].

In the present study, we explored an optimized sample preparation technique and modern LC–MS tools to investigate the metabolism of an old, but front-line anti-tuberculosis (anti-TB) drug, rifampicin (Fig. 1). The drug is associated with many problems including toxicity, potential for interactions with other drugs, variable bioavailability, development of resistance and patient non-compliance. As the drug is used for long period, many of the hurdles are anticipated to be directly or indirectly connected to its metabolism behaviour. Although, metabolic attributes of rifampicin have been studied in various models, including humans [12–18], from the time of its discovery, there are still un-answered questions like: (i) whether metabolism is a reason for its hepatotoxicity? (ii) is the metabolism altered when other drugs are co-administered during therapy? (iii) whether polymorphic enzymes are involved in the drug's variable bioavailability? etc. [19–21]. Due to its long-term use, there is possibility that even trace metabolites accumulate over the period, and result in unexpected adverse outcomes, as previously reported in some classes of compounds [22,23]. Accord-

* Corresponding author. Tel.: +91 172 2214682; fax: +91 172 2214692.
E-mail address: ssingh@niper.ac.in (S. Singh).

0731-7085/$ – see front matter © 2009 Elsevier B.V. All rights reserved.
doi:10.1016/j.jpba.2009.05.009

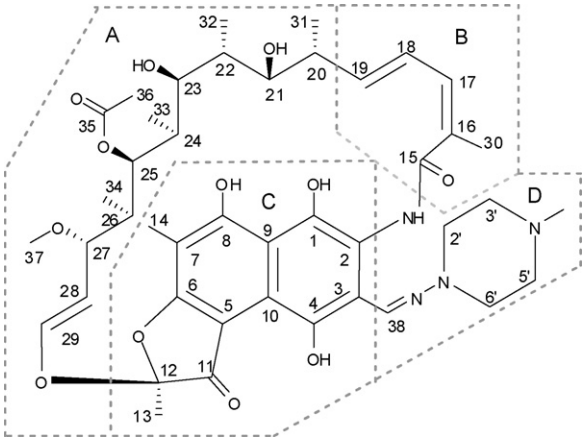

Fig. 1. Structure of rifampicin. Parts A, B, C and D represent aliphatic (saturated), aliphatic (unsaturated), aromatic and piperazine moieties, respectively.

ingly, the basic biotransformation pathways of rifampicin *in vivo* in rat and *in vitro* in various species were revisited using modern approaches of metabolite generation, sample preparation, prediction, detection and characterization. The results are reported in this publication.

2. Experimental

2.1. Chemicals and reagents

Rifampicin was supplied gratis by M/s Panacea Biotec Ltd. (Lalru, India). Testosterone, nicotinamide adenine dinucleotide phosphate reduced (NADPH) tetrasodium salt, sodium carboxy methyl cellulose, di-potassium hydrogen phosphate and potassium phosphate monobasic were purchased from Himedia Laboratories (Mumbai, India). Sprague–Dawley (SD) rats were procured from central animal facility, NIPER (SAS Nagar, India). Human, rat and mouse liver microsomes (HLM, RLM and MLM, respectively) were purchased from BD Biosciences (Woburn, MA, USA). HPLC grade acetonitrile (ACN) was procured from J.T. Baker (Phillipsburg, NJ, USA). 25-Desacetylrifampicin, rifampicin quinone, rifampicin *N*-oxide and 3-formylrifamycin were supplied by Lupin Ltd., Pune, India. Spectroscopic grade deuterated water (D_2O) and acetonitrile (CD_3CN) used in HDE-MS experiments were procured from Sigma–Aldrich (St. Louis, MO, USA). Pure water was obtained from a water purification unit (Elga Ltd., Bucks, England). All other chemicals were of analytical-reagent grade.

2.2. Mass fragmentation studies on rifampicin

MS^n studies were performed on LXQ linear ion-trap equipment (Finnigan Mat, San Jose, USA) controlled with Xcalibur (version 2.0) software. For MS^n studies, 5 μg ml^{-1} solution of the drug was directly injected at a flow rate of 10 μl min^{-1} and the MS parameters were optimized to get best possible fragmentation with acceptable sensitivity. HR-MS studies were carried out using a LC–MS/TOF instrument, which comprised of 1100 series HPLC system from Agilent Technologies (Waldbronn, Germany) and MicrOTOF-Q spectrometer from Bruker Daltonic (Bremen, Germany). The two were operated using combined software comprising of Hystar (version 3.1) and MicrOTOF Control (version 2.0). The response of the LC–MS/TOF system for HR-MS studies was optimized using a 5 μg ml^{-1} drug solution, which was injected directly at a flow rate of 3 μl min^{-1}. The calibration solution used for accurate mass studies was ES Tuning Mix solution (Agilent Technologies, Waldbronn, Germany). All masses were corrected by the internal reference ions having m/z values of 322.04812, 622.02896 and 922.00980 corresponding to $C_6H_{19}O_6N_3P_3$, $C_{12}H_{19}O_6N_3P_3F_{12}$ and $C_{18}H_{19}O_6N_3P_3F_{24}$, respectively. The HDE-MS experiments were carried out by direct injection of the drug solution prepared in D_2O:CD_3CN (70:30). The mass fragmentation studies were also complemented with *in silico* tool, *i.e.*, Frontier 5.1 (Finnigan Mat, San Jose, USA).

2.3. Preparation of rat liver S9 fraction

All the experiments on animals were carried out in accordance with the protocol approved by Institutional Animal Ethics Committee (IAEC/07/64). Male SD-rats (6-week old) of 250 ± 20 g weight (n = 5) were adapted to normal laboratory conditions (12 h dark/12 h light cycles) with free access to drinking water, and to a conventional diet for 1 week. The liver S9 fraction was then prepared, as described in the literature [24], but with some modifications. On a scheduled day, the animals (n = 3) were first anaesthetized with diethyl ether. They were then placed on an operating board ventral side up. A large U-shaped incision was made on the ventral surface exposing the abdominal cavity all the way to the diaphragm. The cut began at the mid-section of the lower abdomen and progressed up toward the right and left foreleg. The intestine was gently lifted and moved over-and-out of the body cavity to the right side of the animal. The liver was perfused *in situ* with ice-cold normal saline. This was then excised, sliced and homogenized in four volumes (w/v) of ice-cold 100 mM phosphate buffer (pH 7.4). The homogenate was centrifuged (9000 × *g*, 10 min) at 4 °C to remove cell debris, mitochondria and nuclei. The resultant supernatant (S9 fraction) was stored in 15 ml centrifuge tubes at −80 °C until use. The protein content of the S9 fraction was estimated using the classical Lowry method [25].

2.4. In vitro metabolite generation

All the below given studies were performed in a single 24-well plate, following the reported methodology [24]. 50 μl of RLM, HLM and MLM suspensions (20 mg ml^{-1}) were placed in three different wells, each containing 845 μl of 100 mM phosphate buffer (pH 7.4). After preconditioning the plate in an incubator shaker for 5 min at 37 °C, 5 μl of 2 mM stock solution of drug was added to each well. Further, 100 μl of 10 mM NADPH (cofactor) was added to start the reaction. In another three wells, control mixtures were taken, which contained phosphate buffer instead of the cofactor. The same protocol was simultaneously followed for rat liver S9 fraction, except that the drug solution was directly added into 895 μl of 1 mg ml^{-1} liver fraction (in phosphate buffer). The viability of *in vitro* systems was evaluated using testosterone, which was treated in the same manner as the drug, but at a final concentration of 200 μM. Subsequently, in each case, the solutions were divided into two parts. One aliquot of 200 μl was withdrawn as a zero time sample and was quenched immediately by the addition of an equal volume of chilled ACN, followed by vortexing. The second aliquot of 800 μl was incubated at 37 °C with a continuous shaking (75 rpm) for 2 h, and then processed similar to the first aliquot. The samples were then centrifuged at 9000 × *g* for 10 min and the supernatants were stored at −20 °C until analysis.

2.5. In vivo metabolism

For *in vivo* metabolism studies, male SD-rats (n = 5) were fasted for 12 h before the experiment. Food and water were provided *ad libitum* after 2 h of the dosing. 50 mg kg^{-1} of the drug was administered as a water suspension, using sodium carboxy methyl cellulose as a suspending agent. The blood samples were collected (∼0.5 ml)

at different time points, *i.e.*, pre-dose, 0.25, 0.50, 1, 2, 4, 8, 12, 24, 48 and 72 h. Plasma was separated from the blood by centrifuging it for 10 min at 9000 × *g*. Another set of animals ($n = 5$) was kept in metabolic cages for urine and feaces collection. After initial acclimatization for 2 h in the cages, the animals were dosed similarly and the samples were collected from the metabolic cages before dosing and 0–4, 4–8, 8–12, 12–24, 24–48, and 48–72 h post-dose. The samples of plasma, urine and faeces, collected across animals and time points (0–72 h), were pooled together to generate a single sample of each matrix. These pooled samples were stored at −20 °C until analyses.

2.6. Preparation of samples for analysis

To obtain concentrated samples free or almost free of biological matrix, the sample preparation method involved protein-precipitation and solid-phase extraction (SPE), as described in the literature [26]. An additional step of freeze-liquid separation was introduced in-between to reduce the loss of polar analytes due to overloading of SPE cartridges. The optimized method is summarized in Fig. 2.

First, ACN up to three times of the aqueous volume was added to the samples, except faeces. In case of feaces, water equivalent to three times the weight of the sample was added, the mixture was vortexed to slurry, and ACN was added three times by volume. The samples were then vortexed and centrifuged for 10 min at 9000 × *g*. The supernatants were subjected to freezing at −20 °C till both ACN and aqueous layers became immiscible, and water layer was frozen. The upper ACN layer, which contained most of the drug and non-polar metabolites were collected in another set of tubes. The lower aqueous layer containing polar metabolites and lesser concentration of the drug and non-polar metabolites were subjected to SPE using HLB® cartridges (Waters, USA). The procedure involved cartridge conditioning with 1 ml methanol followed by 2 ml water, loading of samples (1 ml), washing with 1 ml water and elution of the analytes with 0.5 ml ACN. Finally, aliquots from SPE were pooled with the previously collected ACN layers for a single LC–MS/TOF injection. The mixtures were dried at 40 °C using a nitrogen evaporator (Turbovap, Caliper, USA), and the dried samples were reconstituted in 40 μl diluent (ACN:H_2O, 70:30). In the case of testosterone, the ACN precipitated samples were directly analyzed without further enrichment.

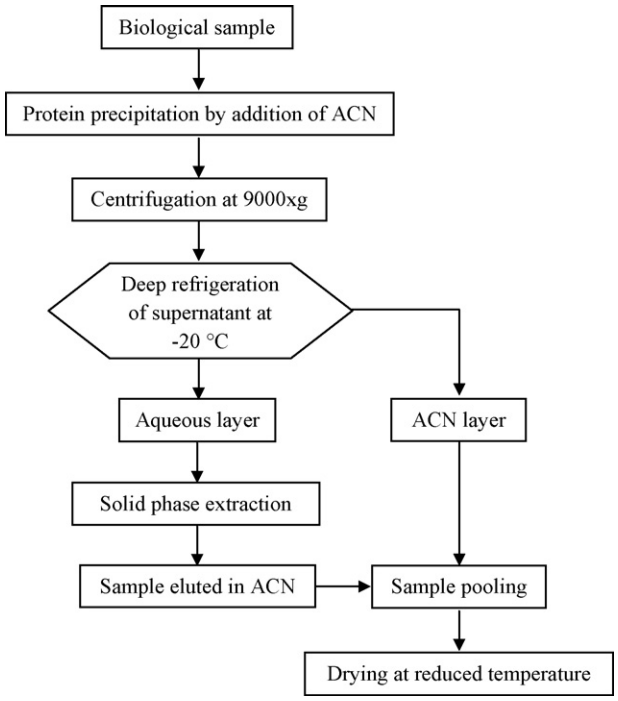

Fig. 2. Schematic representation of an optimized sample preparation approach used for processing of biological samples containing rifampicin and its metabolites.

2.7. Development of LC–UV/DAD method of separation

For the characterization of metabolites by LC–MS/TOF, an HPLC method was first developed using a solution mixture containing rifampicin and its known metabolite or degradant standards including 25-desacetylrifampicin, rifampicin *N*-oxide, 3-formylrifamycin and rifampicin quinone. The mixture was injected into an HPLC system (Waters, USA) consisting of 600 pump, 717 autosampler, 996 PDA detector and millennium software (version 2.1). The separation was achieved on a Zorbax C-18 column (250 mm × 4.6 mm, 5 μm) purchased from Agilent Technologies (Wilmington, DE, USA). To achieve optimal separation, gradient mode was explored taking a mobile phase composed of ACN and 10 mM ammonium acetate. The flow rate, detection wavelength and column temperature were 0.8 ml min^{-1}, 254 nm and 25 °C, respectively.

Testosterone metabolism samples were analyzed using same chromatographic conditions, except that the mobile phase was used in an isocratic mode (ACN:10 mM ammonium acetate, 51:49 v/v), while detection wavelength was 241 nm.

2.8. LC–MS/TOF characterization of metabolites

The drug was first subjected to *in silico* metabolite prediction through Metabolite Predict software available with LC–MS/TOF system. The predictions were carried out up to second generation, involving all mammalian phase I and phase II enzyme systems. The predicted structures were listed along with accurate theoretical mass of their protonated and unprotonated species. Then the developed gradient LC method was extended to LC/DAD–MS/TOF for the characterization of metabolites present in the reconstituted samples (Section 2.7). After passage through DAD, one-fourth of the LC flow was diverted to the mass source. Both ESI positive and negative modes were used to get maximum information on accurate mass and fragmentation of the components. The blank, pure drug and *in vitro* control samples were analyzed similarly. The metabolites were detected in experimental samples (both *in vitro* and *in vivo*) through the help of Metabolite Detection software, which allowed matching of the accurate mass of metabolites eluted during LC–MS/TOF study with those predicted. The software-predicted/detected metabolites and those additionally observed in total ion and UV chromatograms were confirmed through the use of accurate mass values, ring plus double bonds (RDBs) calculations, application of nitrogen rule, and determination of exact mass losses. The site of change in the drug structure as a result of metabolism was identified through comparison of MS fragmentation pattern of each metabolite with that of the drug.

2.9. Post-run semi-quantitative estimation of metabolites from extracted ion chromatograms

After determining structures of metabolites detected in different *in vitro* and *in vivo* samples, extracted ion chromatograms (EICs) of the individual metabolites were evaluated to determine relative (LC–MS-based) amounts of the metabolites. Metabolite levels in the various matrices were expressed as a percent of desacetylrifampicin (M3), a known major metabolite of rifampicin.

3. Results and discussion

3.1. Mass fragmentation behaviour of rifampicin

Fig. 3 shows MS spectra of rifampicin in an ESI positive mode. As shown, mass fragmentation of protonated drug ($M+H^+ = 823$) resulted only two stable fragments of m/z 791 and 399. Several other peaks were detected on zooming the spectra. MS^n ($n = 8$) data were obtained using an ion-trap MS system to understand the sequential order in which the respective product ions were generated. The HR-MS data obtained on LC–MS/TOF analyses of all the fragment ion peaks are given in Table 1. Both HR-MS and MS^n studies were used to derive molecular formulae, and to assign elemental composition to the losses. Additionally, the RDBs and nitrogen rule were applied in assigning possible structures to the fragments. As the drug contained labile hydrogens containing groups (–OH, –NHR, etc.), HDE-MS studies were also carried out to determine the number of exchangeable hydrogen available in the protonated fragments. The HDE-MS spectrum for rifampicin is shown in Fig. 4. The sites of protonation were located based on the HDE behaviour of the fragments and by following the fundamental that onium cations are labile and exhibit HDE, while carbocations do not. Based on all these, a comprehensive mass fragmentation profile of rifampicin was constructed, which is outlined in Fig. 5. *In silico* studies using Frontier 5.1 provided additional support in elucidating mass fragments and their mechanism of formation.

It is proposed that rifampicin initially undergoes simultaneous ionization into multiple fragments of m/z 807, 805, 791, 781, 667 and 519 on loss of CH_4, H_2O, CH_3OH, CH_2CO, and piperazine and aliphatic moieties (parts A + B in Fig. 1), respectively. Of these, except m/z 807 and 519, all other fragments underwent further ionization to yield product ions. The fragments of m/z 805 and 781 lost CH_2CO and H_2O, respectively, and yielded a common ion of m/z 763, which on further H_2O loss generated a fragment of m/z 745. The fragment without piperazine moiety (m/z 667) simply lost H_2O to yield an ion of m/z 649. Otherwise, majority of product ions got generated from a stable fragment of m/z 791. The latter underwent parallel fragmentation on loss of –NR and H_2O to ions of m/z 676 and 773, respectively (Fig. 5). Further ionization of m/z 676 followed the scheme m/z 658 → m/z 616 → m/z 598 → m/z 580. The ion of 773 was proposed to be formed on liberation of water from 21C position, which should be less favoured from stable aromatic side or from 23C position due to intermolecular H-bonding and steric hindrance. The ion underwent further fragmentation by three parallel routes. The first route involved loss of CH_2CO to form an ion of m/z 731, which sequentially lost water to generate fragments of m/z 713 → m/z 695. In the second pathway, there was direct loss of water to form a fragment of m/z 755. The third route involved ring cleavage, resulting in a stable fragment of m/z 399 (seen in the unzoomed spectrum, Fig. 3), a quinone moiety of m/z 397, and an aliphatic part (parts A + B, Fig. 1) with m/z 375. In the HDE spectrum, there were two peaks for the aliphatic structures originating from the ring cleavage, *i.e.*, m/z 375 and 376. This partial HDE occurred due to the intermolecular H-bonding between alcohol moiety attached to 23C and carbonyl oxygen of the acetyl group attached to 25C [27]. The removal of CH_2CO from m/z 375 resulted into fragment of m/z 333, which in deuterated solvent showed two peaks at m/z 334 and 335, again due to the partial HDE, thus confirming its keto-enol structure. The loss of water moiety from m/z 333 resulted into fragment of m/z 315, which showed two peaks of m/z 315 and 316 in the HDE-MS spectrum due to the presence of keto-enol tautomerism. Further, sequential water losses from m/z 315 resulted in fragments of m/z 297 and 279, respectively, where formation of conjugate dou-

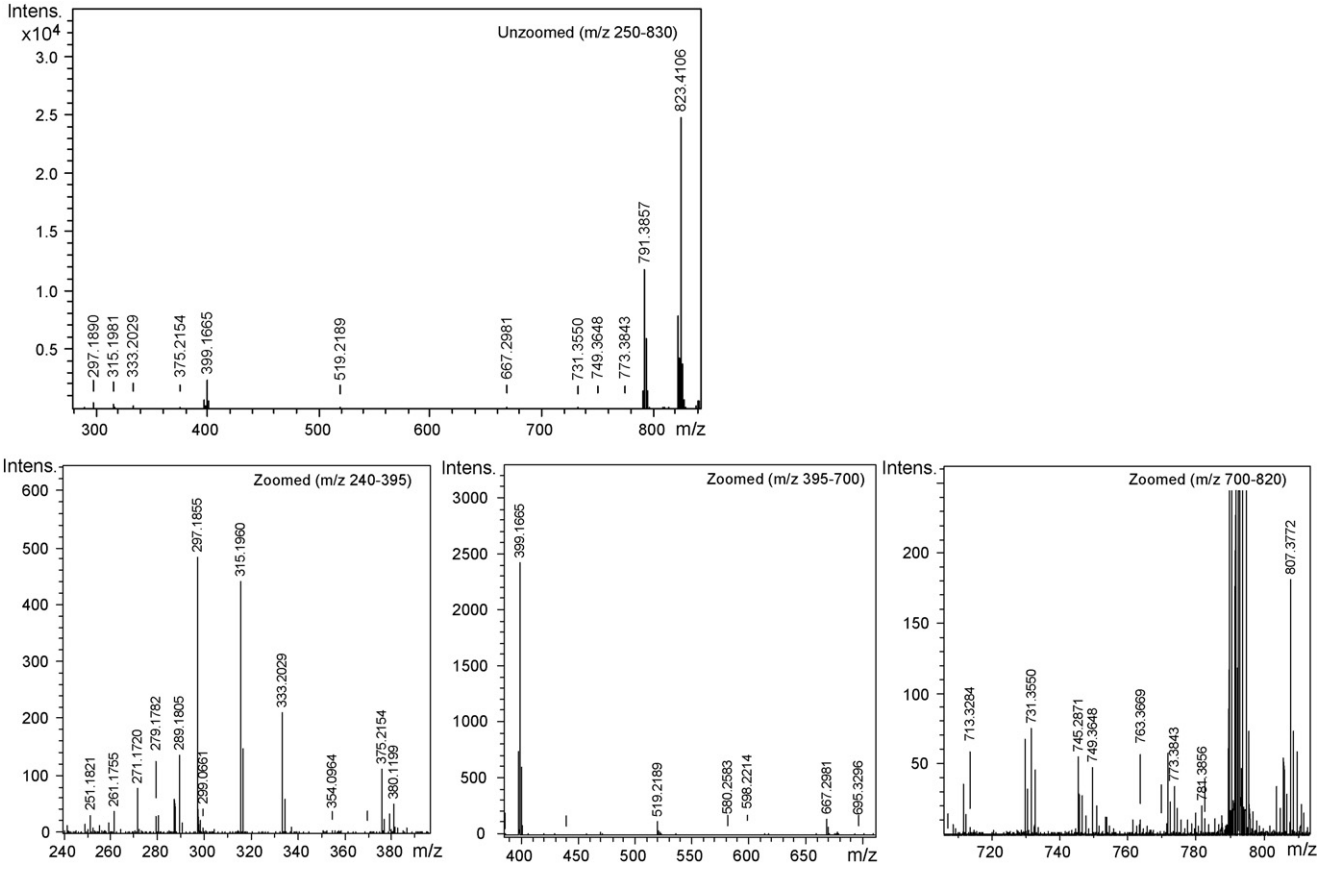

Fig. 3. MS spectra of rifampicin in ESI positive mode.

Table 1
LC–MS/TOF data for rifampicin in ESI positive mode.

Experimental mass	Theoretical mass	Error (ppm)	Number of nitrogens	RDBs	Molecular formula
823.4106	823.4124	2.19	Even or zero	16.5	$C_{43}H_{59}N_4O_{12}^+$
807.3811	807.3801	1.23	Even or zero	17.5	$C_{42}H_{55}N_4O_{12}^+$
805.4038	805.4018	2.48	Even or zero	17.5	$C_{43}H_{57}N_4O_{11}^+$
791.3857	791.3862	0.62	Even or zero	17.5	$C_{42}H_{55}N_4O_{11}^+$
781.3896	781.4018	15.61	Even or zero	15.5	$C_{41}H_{57}N_4O_{11}^+$
773.3843	773.3756	11.25	Even or zero	18.5	$C_{42}H_{53}N_4O_{10}^+$
763.3852	763.3913	7.99	Even or zero	16.5	$C_{41}H_{55}N_4O_{10}^+$
731.3550	731.3651	13.76	Even or zero	17.5	$C_{40}H_{51}N_4O_9^+$
713.3454	713.3545	12.76	Even or zero	18.5	$C_{40}H_{49}N_4O_8^+$
695.3454	695.3439	2.16	Even or zero	19.5	$C_{40}H_{47}N_4O_7^+$
676.2710	676.2752	6.21	Odd	17.5	$C_{37}H_{42}NO_{11}^+$
667.2988	667.3126	20.68	Even or zero	19.5	$C_{38}H_{43}N_4O_7^+$
658.2574	658.2647	11.09	Odd	18.5	$C_{37}H_{40}NO_{10}^+$
649.2982	649.3021	6.01	Even or zero	20.5	$C_{38}H_{41}N_4O_6^+$
616.2496	616.2541	7.30	Odd	17.5	$C_{35}H_{38}NO_9^+$
598.2369	598.2435	11.03	Odd	18.5	$C_{35}H_{36}NO_8^+$
580.2430	580.2330	17.23	Odd	19.5	$C_{35}H_{34}NO_7^+$
519.2189	519.2238	9.44	Even or zero	15.5	$C_{28}H_{31}N_4O_6^+$
399.1665	399.1663	0.50	Even or zero	11.5	$C_{20}H_{23}N_4O_5^+$
397.1511	397.1506	1.26	Even or zero	12.5	$C_{20}H_{21}N_4O_5^+$
382.1404	382.1397	1.83	Odd	12.5	$C_{20}H_{20}N_3O_5^+$
381.1349	381.1319	7.87	Odd	13.0	$C_{20}H_{19}N_3O_5^{\bullet+}$
380.1199	380.1241	11.05	Odd	13.5	$C_{20}H_{18}N_3O_5^+$
379.1145	379.1163	4.75	Odd	14.0	$C_{20}H_{17}N_3O_5^{\bullet+}$
375.2154	375.2166	3.20	Even or zero	7.5	$C_{22}H_{31}O_5^+$
370.1412	370.1397	4.05	Odd	11.5	$C_{19}H_{20}N_3O_5^+$
354.1084	354.1084	0.00	Odd	12.5	$C_{18}H_{16}N_3O_5^+$
333.2029	333.2060	9.42	Even or zero	6.5	$C_{20}H_{29}O_4^+$
315.1960	315.1955	1.68	Even or zero	7.5	$C_{20}H_{27}O_3^+$
299.0661	299.0662	0.33	Even or zero	11.5	$C_{15}H_{11}N_2O_5^+$
297.1855	297.1849	1.99	Even or zero	8.5	$C_{20}H_{25}O_2^+$
279.1782	279.1743	13.97	Even or zero	9.5	$C_{20}H_{23}O^+$

Key: Formulae shown in italics were also observed in Frontier 5.1.

ble bond systems was favoured. The fragmentation of ion of *m*/*z* 399 yielded several small fragments of *m*/*z* 382, 381, 380, 379, 370, 354 and 342 and one prominent peak of *m*/*z* 299. Further fragmentation of the latter resulted in ions of *m*/*z* values 281, 271, 257 and 215, as shown in Fig. 5.

The mass fragmentation behaviour of rifampicin in ESI negative mode was also worked out, where some of the fragment structures corresponded to the mass ionization of the drug in the positive mode (Table 1). However, additional fragments were also found to be present (Table 2), whose structures were elucidated based on HR-MS data (Fig. 6).

3.2. Analysis of testosterone metabolism samples

The activity of *in vitro* models was assessed by HPLC analysis of a well known metabolism prone compound, testosterone. As shown in Fig. 7, all the *in vitro* matrices showed extensive metabolic degradation of testosterone within 2 h.

3.3. Chromatographic separation of rifampicin metabolites

Good separation among the drug and available pure metabolites was achieved on LC–UV/DAD analysis, using the optimized conditions summarized in Table 3. The relative retention times (RR_T) for 25-desacetylrifampicin, 3-formylrifamycin, rifampicin quinone and rifampicin *N*-oxide were 0.64, 1.29, 1.39 and 0.94, respectively, with respect to the drug. Nearly same chromatographic separation was achieved on extension of the method to LC–MS/TOF (Fig. 8a), wherein acceptable separation was also observed among known and unknown metabolites in the reconstituted samples. LC–UV and base peak chromatograms (BPCs) of metabolite samples in complex *in vivo* matrices are shown in Fig. 8.

3.4. In silico prediction of metabolites of rifampicin

In total, 1780 metabolites of rifampicin were predicted up to the second generation, which included all the possibilities of mam-

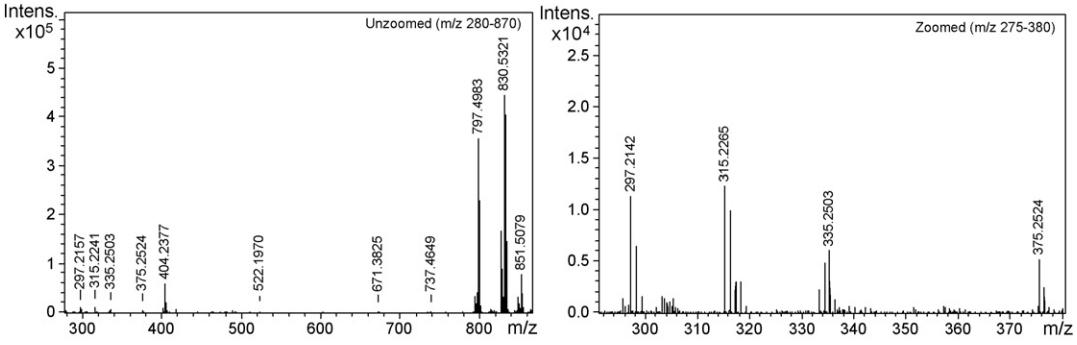

Fig. 4. HDE-MS spectra of rifampicin in ESI positive mode.

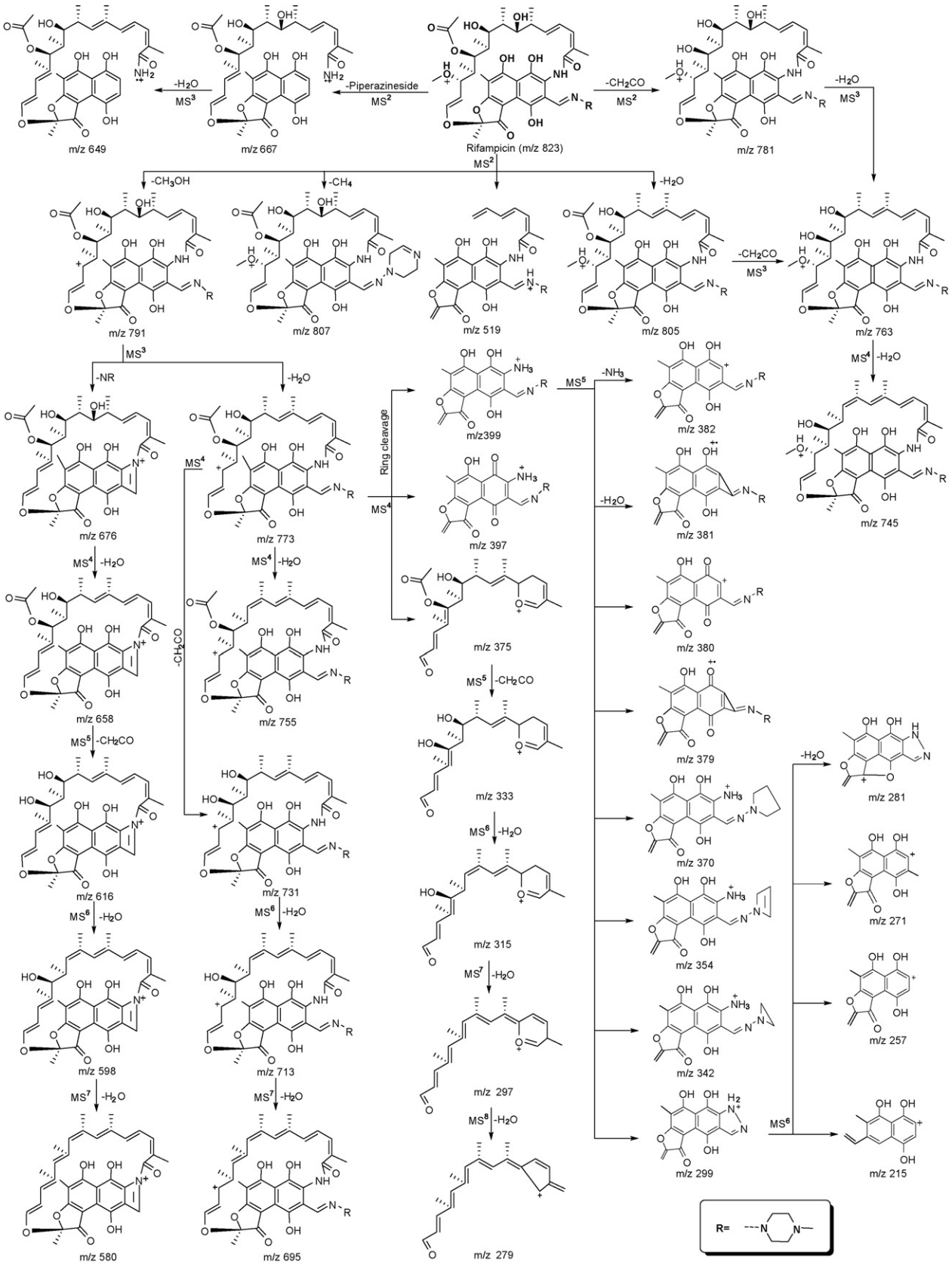

Fig. 5. MS fragmentation pattern of rifampicin in ESI positive mode.

Table 2
LC–MS/TOF data of characteristic fragments of rifampicin in ESI negative mode.

Experimental mass	Theoretical mass	Error (ppm)	RDBs	Molecular formula
722.3032	722.3056	3.32	17.0	$C_{38}H_{46}N_2O_{12}^{\bullet -}$
708.3070	708.3025	6.35	16.5	$C_{38}H_{46}NO_{12}^{-}$
690.2767	690.2794	3.91	18.0	$C_{37}H_{42}N_2O_{11}^{\bullet -}$
663.2949	663.2923	3.92	16.5	$C_{36}H_{43}N_2O_{10}^{-}$
630.2549	630.2583	5.39	18.0	$C_{35}H_{38}N_2O_9^{\bullet -}$
626.2567	626.2508	9.42	19.5	$C_{35}H_{36}N_3O_8^{-}$
606.2629	606.2701	11.88	16.0	$C_{32}H_{38}N_4O_8^{\bullet -}$
519.2171	519.2249	15.02	15.5	$C_{28}H_{31}N_4O_6^{-}$
490.1792	490.1745	9.59	16.0	$C_{27}H_{26}N_2O_7^{\bullet -}$
420.1248	420.1327	18.80	15.0	$C_{23}H_{20}N_2O_6^{\bullet -}$

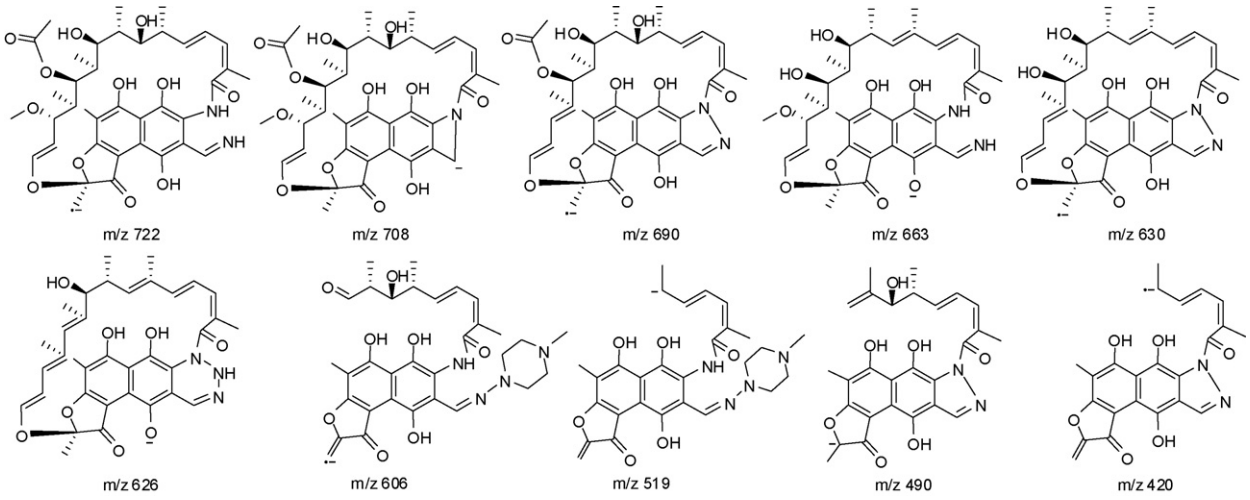

Fig. 6. Characteristic MS fragments of rifampicin in ESI negative mode.

Table 3
Optimized parameters for LC–MS/TOF and MS^n studies.

HPLC parameters	Column: Zorbax C-18 (250 mm × 4.6 mm, 5 μm) (Agilent Technologies, USA) Mobile phase: ACN (A) and 10 mM ammonium acetate (B) Flow rate: 0.8 ml min^{-1} Detection wavelength: 254 nm Gradient program: %A = 20–30% (0–22 min), 30–40% (22–38 min), 40–60% (38–50 min), 60–80% (50–60 min), 80% (60–65 min), 80–20% (65–70 min), 20% (70–80 min)		
MS-TOF parameters		ESI +ve mode	ESI −ve mode
	End plate offset	−500 V	−500 V
	Capillary	+4500 V	+4500 V
	Nebulizer	1.2 Bar	1.2 Bar
	Dry gas	6 l min^{-1}	6 l min^{-1}
	Dry temperature	200 °C	200 °C
	Funnel 1 RF	200 Vpp	200 Vpp
	Funnel 2 RF	300 Vpp	200 Vpp
	ISCID energy	0 eV	10 eV
	Hexapole RF	300 Vpp	300 Vpp
	Ion energy	5 ev	5 eV
	Low mass	300 *m/z*	300 *m/z*
	Collision energy	18 eV/z	30 eV/z
	Transfer time	100 μs	100 μs
	Collision RF	400 Vpp	400 Vpp
	Pre-pulse storage	10 μs	10 μs
	Detector voltage	−1200 V	−1200 V
MS^n parameters	Spray voltage	4.75 kV	
	Capillary temperature	250 °C	
	Vaporizer temperature	200 °C	
	Helium gas flow rate	0.5 ml min^{-1}	
	Scan rate for product ions	11,000 amu s^{-1}	

Table 4
Rifampicin metabolites detected in test samples against *in silico* predicted first generation metabolites.

Metabolite type	Molecular weight	Number of metabolites predicted	Number of metabolite detected
Mono-oxygenated rifampicin	838.40	21	9
Desacetylrifampicin	780.39	1	1
Rifampicin quinone	820.38	2	2
Demethylrifampicin	808.38	2	2
Rifampicin glucuronide	998.44	7	1

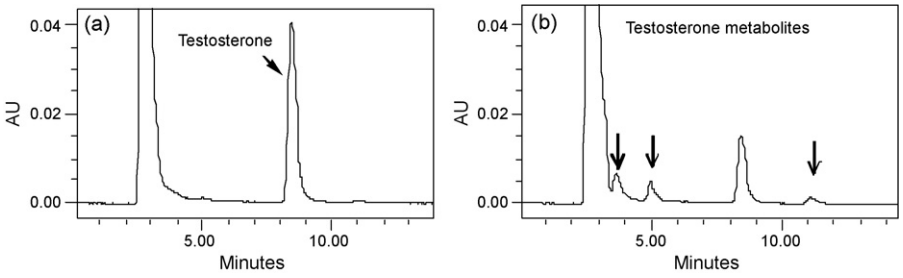

Fig. 7. LC–UV chromatograms of testosterone *in vitro* samples incubated without and with NADPH (a and b, respectively).

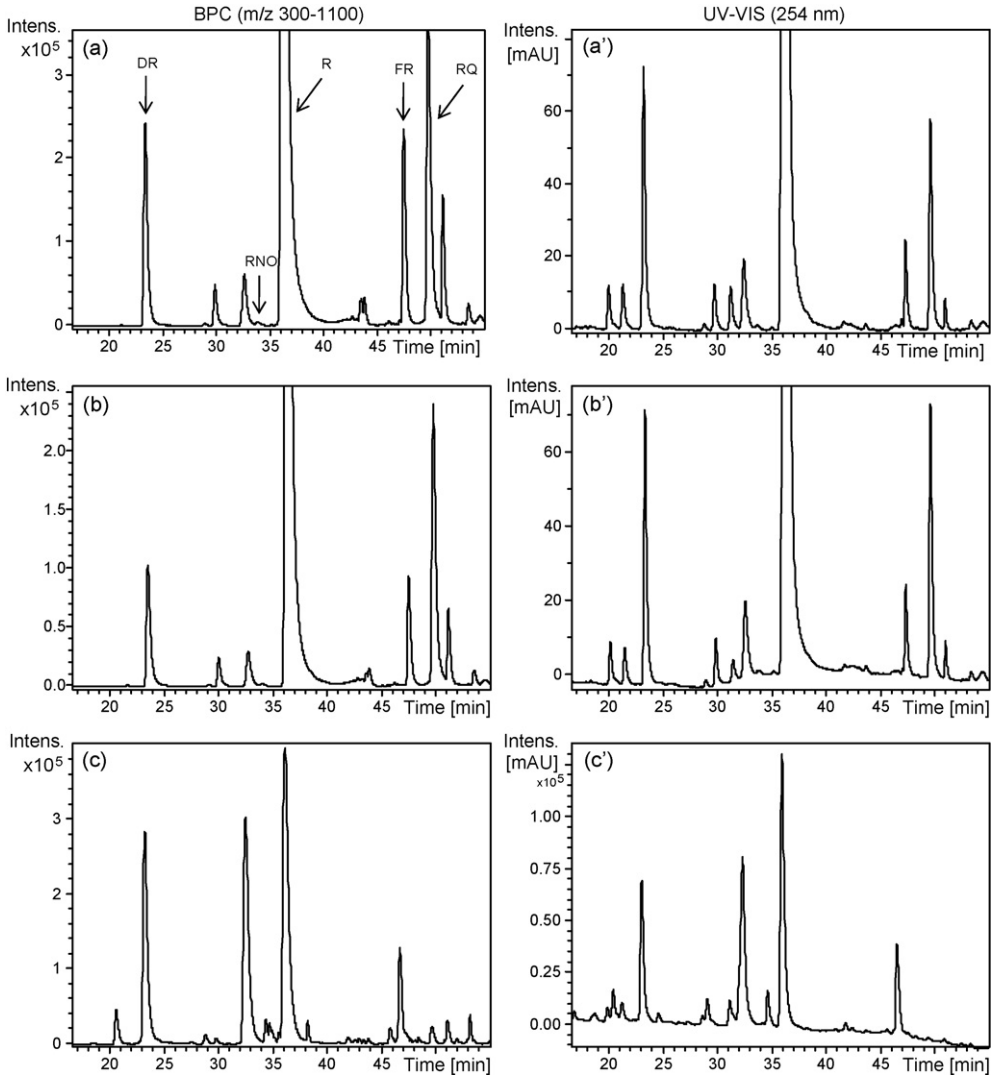

Fig. 8. Typical LC–UV and base peak chromatograms of rifampicin metabolites in plasma (a and a′), urine (b and b′) and feaces (c and c′) samples. Key: R = rifampicin, DR = 25-desacetylrifampicin, FR = 3-formylrifamycin, RQ = rifampicin quinone, and RNO = rifampicin *N*-oxide.

Table 5
LC–MS/TOF data of rifampicin and its metabolites.

Drug/metabolites	RR_T	Experimental mass (error in ppm)		Molecular formula	Metabolic change[a]
		ESI +ve mode	ESI −ve mode		
Drug	1.00	823.4106 (2.2)	821.3988 (1.2)	$C_{43}H_{58}N_4O_{12}$	–
M1	0.52	797.3948 (2.4)	795.3881 (7.4)	$C_{41}H_{56}N_4O_{12}$	$-[C_2H_2]$
M2	0.57	767.3830 (0.4)	765.3726 (0.1)	$C_{40}H_{54}N_4O_{11}$	$-[C_3H_4O]$
M3	0.64	781.4040 (2.8)	779.3806 (8.6)	$C_{41}H_{56}N_4O_{11}$	$-[C_2H_2O]$
M4	0.70	839.4158 (10.1)	837.3898 (3.6)	$C_{43}H_{58}N_4O_{13}$	+[O]
M5	0.71	999.4412 (0.3)	997.4345 (1.7)	$C_{49}H_{66}N_4O_{18}$	$+[C_6H_8O_6]$
M6	0.72	839.4012 (7.3)	837.4001 (8.7)	$C_{43}H_{58}N_4O_{13}$	+[O]
M7	0.77	839.4073 (0.0)	837.3936 (1.0)	$C_{43}H_{58}N_4O_{13}$	+[O]
M8	0.80	839.3999 (8.8)	837.3930 (0.2)	$C_{43}H_{58}N_4O_{13}$	+[O]
M9	0.82	823.4139 (1.8)	821.4005 (3.3)	$C_{43}H_{58}N_4O_{12}$	No change
M10	0.90	809.3947 (2.5)	807.3811 (1.4)	$C_{42}H_{56}N_4O_{12}$	$-[CH_3]$
M11	0.93	809.3899 (8.4)	807.3792 (3.7)	$C_{42}H_{56}N_4O_{12}$	$-[CH_3]$
M12	0.94	839.3985 (10.5)	837.3926 (0.2)	$C_{43}H_{58}N_4O_{13}$	+[O]
M13	0.96	684.2990 (3.7)	682.2901 (4.7)	$C_{36}H_{45}NO_{12}$	$-[C_7H_{13}N_3]$
M14	0.98	797.3998 (3.9)	795.3806 (2.0)	$C_{41}H_{56}N_4O_{12}$	$-[C_2H_2]$
M15	1.22	839.4036 (4.4)	837.3973 (5.4)	$C_{43}H_{58}N_4O_{13}$	+[O]
M16	1.28	839.4066 (0.8)	837.3962 (4.1)	$C_{43}H_{58}N_4O_{13}$	+[O]
M17	1.29	726.3084 (5.0)	724.3033 (8.0)	$C_{38}H_{47}NO_{13}$	Unpredicted
M18	1.29	837.3907 (1.2)	835.3820 (5.9)	$C_{43}H_{56}N_4O_{13}$	Unpredicted
M19	1.34	839.4082 (1.1)	837.3962 (4.1)	$C_{43}H_{58}N_4O_{13}$	+[O]
M20	1.39	821.3978 (1.3)	819.3839 (2.1)	$C_{43}H_{56}N_4O_{12}$	$-[H_2]$
M21	1.44	837.3954 (4.4)	835.382 (5.9)	$C_{43}H_{56}N_4O_{13}$	Unpredicted

[a] (+) indicates addition, while (−) indicates loss of the respective moieties.

malian enzyme systems. These were compared with metabolites detected in the test samples (Table 4).

3.5. Accurate mass and fragmentation studies

The accurate mass values of the drug and its metabolites in both positive and negative modes are listed in Table 5, along with their chemical formulae. The table also shows type of metabolic change that was determined from comparison of mass values and chemical formulae of all the metabolites and the drug. As shown, several metabolites had the same mass and chemical formula, *e.g.*, metabolites coded M4, M6–M8, M12, M15, M16 and M19, indicating that there were multiple sites for metabolism by the same route. The formation of more than one metabolites with same molecular mass was also evident from EICs, as shown in Fig. 9a, b, e, g and k. To derive the exact location of the metabolic change in all the cases, fragments with common losses, common fragments, characteristic neutral losses and other important fragments for the drug and metabolites observed in positive ESI mode are listed in Table 6. The key fragments obtained in negative ESI mode are listed in Table 7. Based

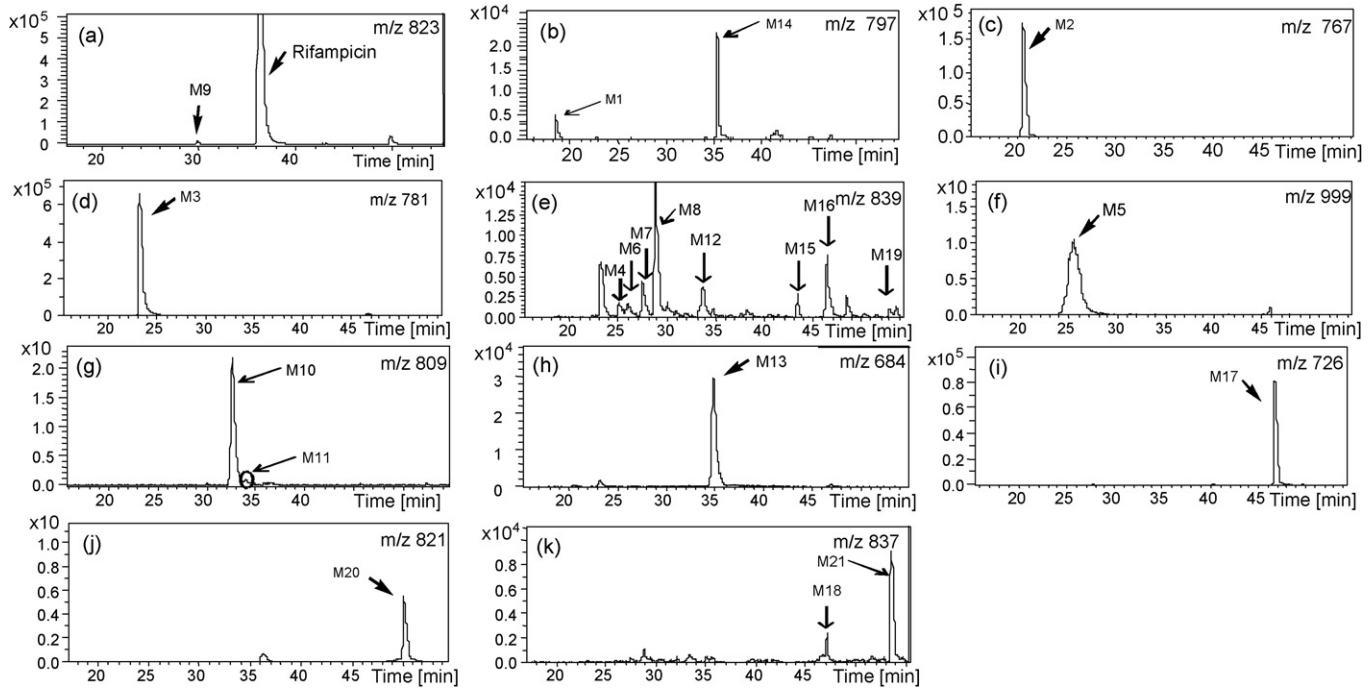

Fig. 9. Typical extracted ion chromatograms of rifampicin and its metabolites observed in biological matrices. This figure shows extracted ion chromatogram of drug and acetylated desacetylrifampicin metabolites (*m/z* 823), monooxygenated desacetylrifampicin (m/z 797), demethyl-desacetylrifampicin (m/z 767), desacetylrifampicin (m/z 781), mono-oxygenated rifampicin (m/z 839), rifampicin glucuronide (m/z 999), demethylrifampicin (m/z 809), desacetyl-3-formylrifamycin (m/z 684), 3-formylrifamycin (m/z 726), rifampicin quinone (m/z 821), and mono-oxygenated rifampicin quinone-1 (m/z 837) (a–k, respectively).

Table 6
Mass fragmentation data of rifampicin and its metabolites in ESI positive mode.

Drug/metabolites	Major fragments with common loss[a]				Characteristic common fragments				Other important fragments	Characteristic neutral losses
	M	M-32	M-50	M-92						
Drug	823	791	773	731	399	375	333	315	807, 781, 763, 676, 667, 658, 616, 598, 519, 299, 297, 279	32, 42, 50, 60, 92
M1	797	765	747		399		331	313	729, 625	32, 50
M2	767	735	717		385		333	315	699, 669, 663, 634, 625, 616, 505, 297	32, 50
M3	781	749	731		399		333	315	763, 634, 625, 616, 598, 519, 299, 297, 279, 271	32, 50
M4	839	807	789	747	399	373	331	313	821, 729	32, 50, 92
M5	999	967			399	375	333	315	823, 791, 773, 731, 676, 667, 658, 616, 519, 299	176, 32
M6	839	807	789	747	415	375	333		821, 397	32, 50, 92
M7	839	807		747	399	373	331		821, 729	32, 92
M8	839	807	789		399	373	331	313	821, 771, 729, 674, 667	32, 50
M9	823	791	773	731	399	375	333	315	807, 676, 667, 658, 616, 519, 299, 297	32, 42, 50, 60, 92
M10	809	777	759	717	385	375	333	315	791,741, 699, 681, 505, 353, 297, 279	32, 50, 92
M11	809				399	375	333		791, 769, 505, 297	42
M12	839	807		747	398	375	333	315	822, 791, 676, 659, 641, 536, 520, 399	32, 92
M13	684	652	634				333		616, 598, 302	32
M14	797	765								32
M15	839	807	789	747						32, 50, 92
M16	839	807	789	748					821, 819	32, 50, 92
M17	726	694	676	634	302	375	333	315	658, 616, 598, 580, 562, 492, 464, 446, 424, 406	32, 50, 92
M18	837	805			399	373	331	313		32
M19	839	807			415					32
M20	821	789	771	729	397	375	333	315	779, 761, 711, 667, 519, 297	32, 42, 50, 60, 92
M21	837	805			413	375		315	731, 535, 665	32

[a] M = molecular ion peak.

Table 7
MS fragmentation data of rifampicin and its metabolites in ESI negative modes.

Drug/metabolites	$[M-H]^-$	Key fragments									
Drug	821	722	708	690	663	631	626	606	519	490	420
M1	795	696	664								436
M2	765	680	666						505		
M3	779	680	664			634		606	519	490	420
M4	837	738	706								436
M5	997	722	708								
M6	837	738	706								436
M7	837	738	706						535		436
M8	837	738	706		679				535		436
M9	821	722	708	690	663	631		606	519		420
M10	807	722	708	690	663	631	626	592	505	476	420
M11	807	708		690	649						
M12	837	722	708		663	631			519		420
M13	682										422
M14	795	722									422
M15	837	724									
M16	837	724									
M17	724	724		692		632					422
M18	835		706								
M19	837	724									
M20	819	720	706		661		624		518	490	418
M21	835		706								

on all the data, structures were elucidated for various metabolites, which were supported by their fragmentation patterns, as shown in Figs. 10–13.

3.6. Types of metabolites formed in the various in vitro and in vivo matrices and their semi-quantitative estimation

By using the optimized sample preparation approach, even the minor and trace-level metabolites were detected. The LC–MS characterized metabolites in the various *in vitro* and *in vivo* matrices and their relative amounts are summarized in Table 8. As the EIC ratios of individual metabolites to the parent drug were very low, particularity in the case of trace-level metabolites, the relative amounts of metabolites were expressed as a percent of EIC of desacetylrifampicin (M3), a known major metabolite of rifampicin. Metabolites with relative ratio >20% were termed as major, between 1 and 20% as minor, and <1% as trace.

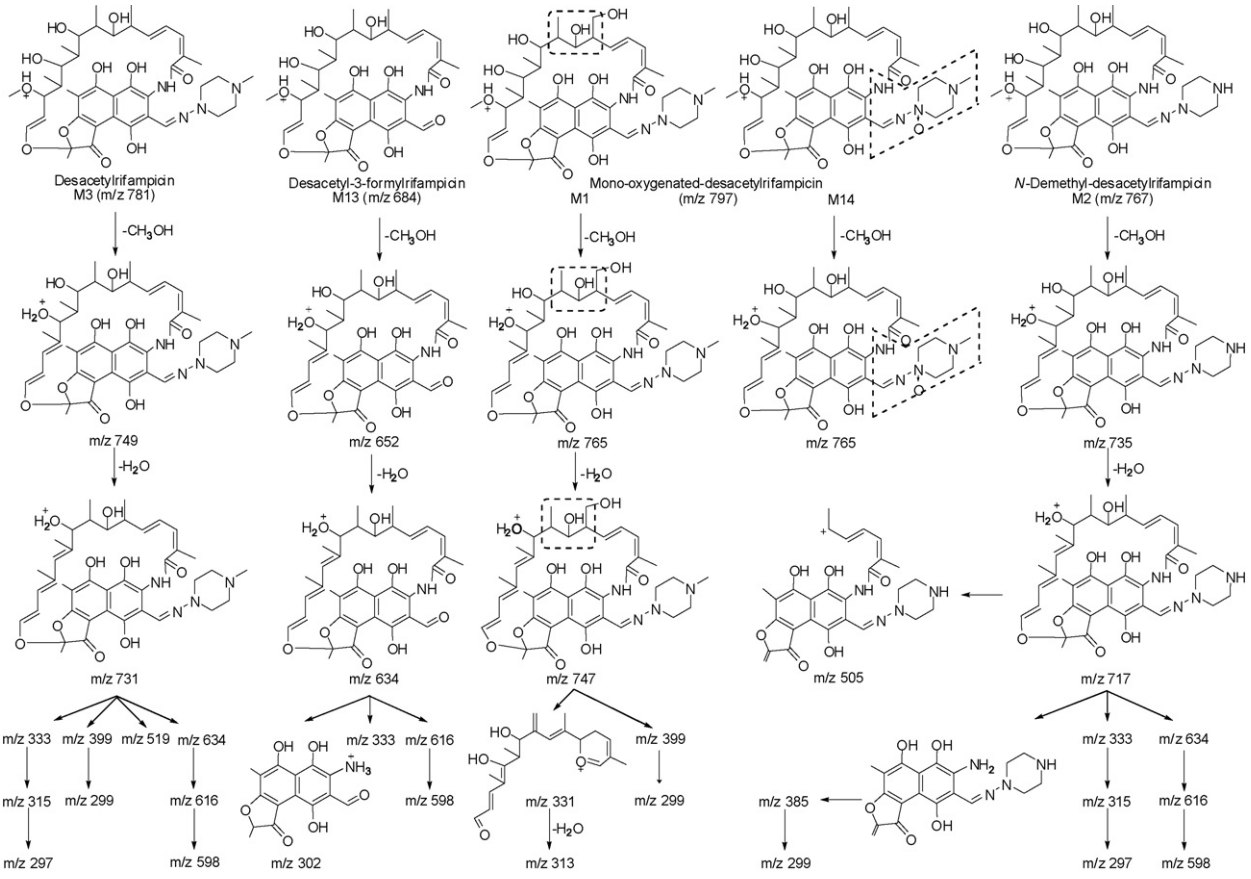

Fig. 10. Characteristic mass fragmentation profiles of desacetylrifamycin and its second generation metabolites in ESI positive mode. Dotted areas indicate postulated sites of oxygenation.

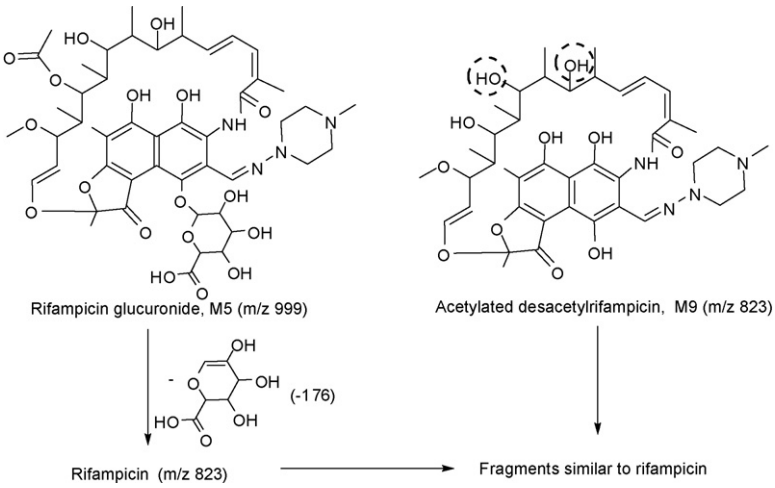

Fig. 11. Characteristic mass fragmentation profiles of conjugated products of rifampicin in ESI positive mode. Encircled areas indicate possible sites of acetylation.

3.7. Structure elucidation of rifampicin metabolites and explanation of their presence in different matrices

Desacetylrifampicin (M3), a known main metabolite of rifampicin [12–18], also appeared as the major peak in this study (Fig. 9d). Its presence was verified by spiking with the standard. The metabolite showed mass of *m*/*z* 781, different by 42 Da than rifampicin, suggesting absence of acetyl (CH_2CO) moiety (Table 5). The same mass difference was observed in other fragments too, *viz.*, *m*/*z* 676 → *m*/*z* 634, *m*/*z* 667 → *m*/*z* 625 and *m*/*z* 658 → *m*/*z* 616 (Table 6, Fig. 10). Also, there was absence of the fragment of *m*/*z* M-92, typical for the loss of $CH_3COOH + CH_3OH$. Also, intense acetyl containing fragments of *m*/*z* 375 or 373 were absent. The outcome was same even from negative ionization mode study, where mass peak of *m*/*z* 680 in M3 corresponded to that of *m*/*z* 722 for the drug (Table 7). This metabolite was prominently formed in all *in vitro* and *in vivo* matrices, in line with the literature reports [12–18].

The other known metabolite, *i.e.*, rifampicin glucuronide (M5) [12], was characterized from mass peak of *m*/*z* 999, and was also justified by its fragmentation pattern (Fig. 11). The accurate mass difference showed addition of $-C_6H_8O_6$ in the molecule, equivalent to the glucuronide moiety. The characteristic neutral loss of 176 Da and appearance of the fragment of *m*/*z* 823 confirmed it to be a conjugated structure. All other fragments were similar to the drug (Tables 6 and 7 and Fig. 11). The glucuronidation was predicted to occur at phenolic OH-group [28], which was preferred to be at 4C position of rifampicin molecule (Fig. 1) because of the anticipated least steric hindrance at this location. The metabolite was present to

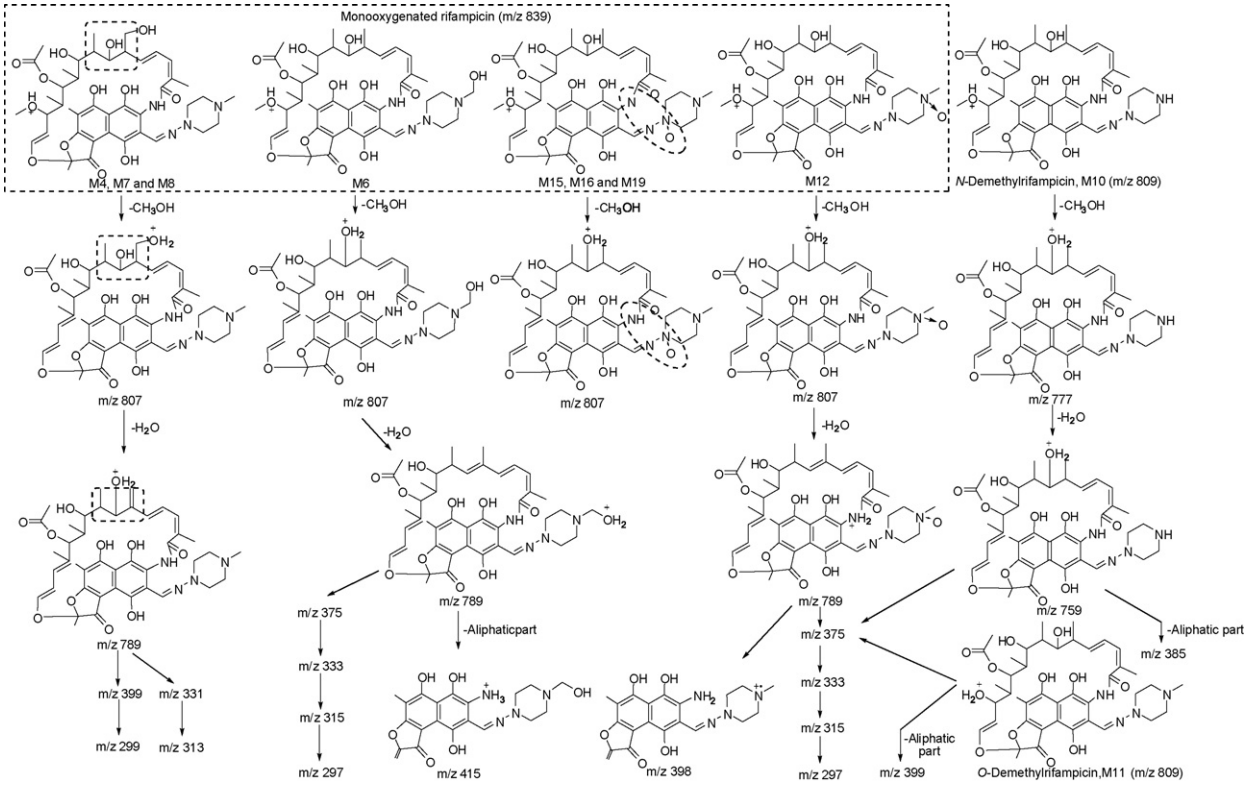

Fig. 12. Characteristic mass fragmentation profiles of mono-oxygenated- and demethylrifampicin-derivatives in ESI positive mode. Dotted areas indicate postulated sites of oxygenation.

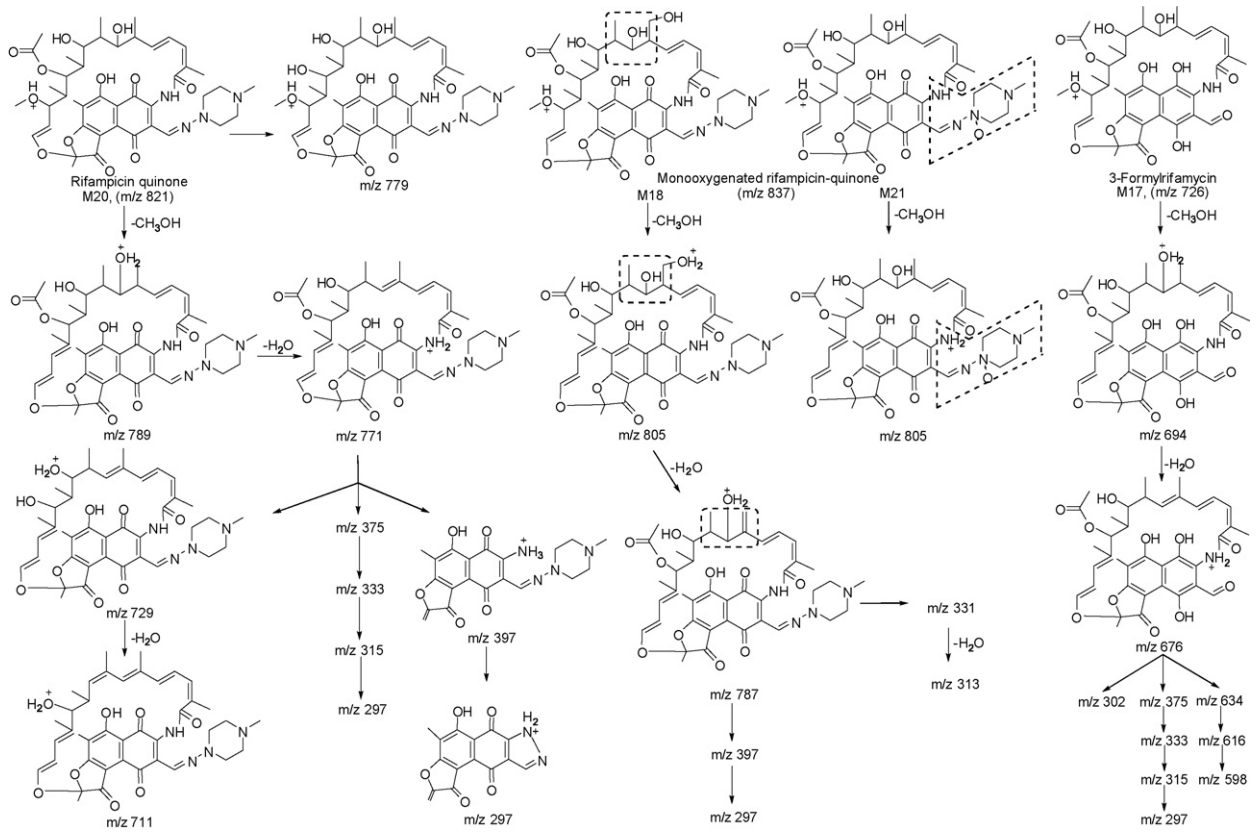

Fig. 13. Characteristic mass fragmentation profiles of rifampicin quinone, its secondary metabolites and 3-formylrifamycin in ESI positive mode.

the maximum in feaces and least in plasma. Being a known metabolite, no phase II *in vitro* metabolism studies were carried out using cofactor uridine-diphospho (UDP)-glucuronic acid.

The metabolite M10 (*m*/*z* 809) eluted earlier to the drug (Fig. 9g), pointing to its higher polarity. As shown in Table 5, there was loss of 14.0157 Da, indicating demethylation of the drug in line with its polarity behaviour. Among the two locations of demethylation in rifampicin (*O*-methyl group at 27C and terminal *N*-methyl group in piperazine moiety), the site of modification in M10 was elucidated by its unique fragmentation pattern in comparison to the

Table 8
LC–MS characterized metabolites of rifampicin following incubation of rifampicin in various *in vitro* systems and following a single oral administration (50 mg/kg) of rifampicin to male SD-rats. The relative amounts of metabolites are expressed as a percent of EIC of desacetylrifampicin.

Metabolite	Code	*In vitro*				*In vivo*		
		RLM	HLM	MLM	R-'S9'	Urine	Feaces	Plasma
Mono-oxygenated desacetylrifampicin-1	M1	√ (L)	√ (L)	√ (L)	√ (L)	x	√ (L)	x
Demethyl-desacetylrifampicin	M2	x	x	x	x	√ (L)	√ (M)	√ (L)
Desacetylrifampicin	M3	√ (H)	√ (H)	√ (H)	√ (H)	√ (H)	√ (H)	√ (H)
Mono-oxygenated rifampicin-1	M4	√ (L)	√ (L)	x	x	x	√ (L)	x
Rifampicin glucuronide	M5	NA[a]	NA[a]	NA[a]	NA[a]	√ (M)	√ (H)	√
Mono-oxygenated rifampicin-2	M6	√ (L)	√ (L)	√ (L)	x	x	√ (L)	√ (L)
Mono-oxygenated rifampicin-3	M7	√ (L)	√ (L)	√ (L)	x	x	√ (L)	√ (L)
Mono-oxygenated rifampicin-4	M8	√ (H)	√ (H)	√ (H)	√ (H)	√ (L)	√ (H)	√ (L)
Acetylated desacetylrifampicin	M9	√ (L)	√ (M)	√ (L)	√ (L)	√ (M)	√ (M)	√ (M)
N-Demethylrifampicin	M10	√ (M)	√ (M)	√ (M)	√ (M)	√	√ (H)	√ (M)
O-Demethylrifampicin	M11	√ (L)	√ (L)	x	x	x	x	√ (L)
Mono-oxygenated rifampicin-5	M12	√ (M)	√ (M)	√ (M)	√ (M)	√ (M)	√ (M)	√ (M)
Desacetyl-3-formylrifamycin	M13	x	x	x	x	x	√ (M)	x
Mono-oxygenated desacetylrifampicin-2	M14	√ (L)	√ (L)	√ (L)	√ (L)	x	√ (M)	x
Mono-oxygenated rifampicin-6	M15	√ (M)	√ (M)	√ (M)	√ (M)	√ (L)	√ (M)	x
Mono-oxygenated rifampicin-7	M16	√ (M)	√ (M)	√ (M)	√ (M)	x	√ (M)	√ (L)
3-Formylrifamycin	M17	√ (L)	√ (L)	√ (L)	√ (L)	√ (M)	√ (H)	√ (H)
Mono-oxygenated rifampicin quinone-1	M18	√ (L)	√ (L)	√ (L)	√ (L)	√ (L)	√ (L)	√ (L)
Mono-oxygenated rifampicin-8	M19	√ (M)	√ (M)	√ (M)	√ (M)	x	√ (M)	x
Rifampicin quinone[b]	M20	√ (H)	√ (H)	√ (H)	√ (H)	√ (M)	√ (L)	√ (M)
Mono-oxygenated rifampicin quinone-2	M21	√ (L)	√ (L)	√ (L)	√ (L)	x	√ (L)	√ (L)

R-'S9' = rat liver S9 fraction; √ = metabolite is present, x = metabolite is absent; H = major metabolite, >20% of M3; M = minor metabolite, 1–20% of M3; L = trace metabolite, <1% of M3.

[a] Not applicable.

[b] Rifampicin quinone is mainly generated by auto-oxidation during *in vitro* incubation and sample processing.

drug (Tables 6 and 7 and Fig. 12). The metabolite showed characteristic peaks of *m*/*z* 385 and 505 corresponding to the drug fragments of *m*/*z* 399 and 519, which clearly indicated that demethylation occurred at the piperazine moiety in the drug (part D in Fig. 1). The same was confirmed even through characteristic neutral losses of 32 and 50 Da representing an intact *O*-methyl group. This metabolite, which is previously known to be formed in minor concentration from rifampicin [13], was found as a major metabolite of the drug in this study. The metabolite appeared in all the matrices, though it was excreted mainly in feaces, where its extent was almost equivalent to desacetylrifampicin (M3) (Table 8).

The metabolite M17 (*m*/*z* 726) was identified in preliminary study to be 3-formylrifamycin, because it eluted at the same retention time as that of the standard (Fig. 9i). Its identification was further confirmed through a spiking study and comparison of fragmentation pattern with the drug (Tables 6 and 7 and Fig. 13). Similar to the drug, the metabolite showed intense fragments of *m*/*z* 676, 658, 616, 598, 375, 333 and 315 in ESI positive mode, depicting no change in the ring and aliphatic part of the drug molecule (parts A + B + C in Fig. 1). Moreover, while the drug showed fragment of *m*/*z* 399 for parts C + D (Fig. 1), the metabolite showed a typical fragment of *m*/*z* 302, resulting from loss of piperazine moiety (part D, Fig. 1). In ESI negative mode, the fragments of *m*/*z* 724, 692 and 422 also proved the same (Table 7). The metabolite was observed in trace quantities in the *in vitro* systems as compared to *in vivo* matrices, which indicated role of non-hepatic enzyme systems, perhaps chemical decomposition. This was substantiated as rifampicin is known to hydrolyse to 3-formylrifamycin (M17) in an acidic environment [29,30]. The order of the presence of M17 in the *in vivo* matrices was faeces > plasma > urine. As 3-formylrifamycin is poorly soluble, only small amount of it was absorbed after *in situ* formation in stomach, and majority of it found its way into faeces.

The metabolite M20 (*m*/*z* 821) was identified as rifampicin quinone on comparison of chromatographic profile with the standard. Accurate mass studies revealed the difference of two hydrogens (2.0157) in the structure, as compared to the drug. The intense peak of *m*/*z* 397 as compared to *m*/*z* 399 in the drug (Table 6 and Fig. 13), confirmed the change at parts C + D (Fig. 1). The formation of M20 was intense in the *in vitro* samples as compared to *in vivo* in feaces, plasma and urine. However, M20 was also observed in the *in vitro* control mixtures without the cofactor. This indicated that in the *in vitro* system, apart from metabolism, there was oxidation of drug [31] during incubation and shaking at 37 °C for 2 h. So, although it appeared to be a major metabolite in final samples, it perhaps was formed by chemical degradation of rifampicin.

Regarding the minor metabolites M1, M2, M4, M6–M9, M11–16, M18, 19 and M21, most of them were characterized to be mono-oxidation products of rifampicin. The metabolite M1 eluted earliest in the chromatogram (Fig. 9b) and was hence the most polar of all. It was found to have *m*/*z* value of 797. The comparison of the accurate mass and formula of the drug with the metabolite indicated loss of a $-C_2H_2$ moiety (Table 5), which clearly showed that it was not formed directly as a first generation metabolite. Its fragmentation pattern (Table 6) did not show loss of ions of 42 and 92 Da in comparison to the drug, indicating at desacetylation at 25C as one of the changes (Fig. 1). The same was confirmed by the absence of fragments of *m*/*z* 375 or 373 (Table 6 and Fig. 10), which were characteristic of the acetylated structure. The accurate mass studies allowed the postulation that during the second generation process there was addition of oxygen moiety (*m*/*z* 15.9949). The occurrence of oxidation away from parts C + D (Fig. 1) of the molecule was confirmed through the presence of fragment of *m*/*z* 399 (Fig. 10). A fair indication that oxidation occurred at saturated aliphatic side (part A) of rifampicin (Fig. 1) was provided by the presence of fragments of *m*/*z* 331 and 315. The postulation was supported by a reported study on rifabutin, a structural congener of rifampicin, where oxidation at saturated aliphatic side (part A in Fig. 1) was proven through mass and NMR investigations [32]. This metabolite was observed in traces in all *in vitro* systems, while it was detected in slightly higher amounts in feaces. It was not seen in urine and plasma, probably due to low mass abundance during mass studies.

As evident in EIC in Fig. 9b, there was another metabolite with the same mass of *m*/*z* 797, as M1, which eluted beyond at 35 min. The fragmentation pattern of this product (M14) (Table 6 and Fig. 10) exhibited the absence of fragments of *m*/*z* 375 or 373, and neutral losses of 42 and 92 Da, indicating that it was desacetylated like M1. Accurate mass studies showed that it was also an oxidized product, similar to M1 (Table 5). As rifampicin structure (Fig. 1) had only one position (25C) for desacetylation, it indicated that oxidation perhaps occurred at a different site than in M1. As the fragment of *m*/*z* 399 (Fig. 10), characteristic for unchanged aromatic side (parts C + D, Fig. 1), was absent in this case, it indicated that the change occurred at either part C or D. Looking into the chromatographic resolution, it was observed that M1 appeared at 18.8 min, desacetylrifamipicin at 23.1 min, while M14 resolved at 35.8 min. This indicated that M14 was much less polar, though usually there should be an increase in polarity of any compound on addition of oxygen [33,34]. Based on the reverse behaviour reported in the literature for *N*-oxidation products [35–38], oxidation in case of M14 was proposed to take place at nitrogen atoms in part D of the rifampicin molecule (Fig. 1). As desacetylation increased polarity, but the RR_T of M14 was higher than the known 4′*N*-oxide of rifampicin (Fig. 9b), the site of metabolic change in M14 was indicated to happen at different nitrogen atoms in part D (Fig. 1). However, it was not possible to fix exact position of oxidation among the said three nitrogen atoms, as MS fragmentation information was very less for this metabolite. The extent of formation of M14 in different *in vivo* and *in vitro* matrices was parallel to that of M1.

The metabolite M2 (*m*/*z*, 767) eluted at 20.5 min in the chromatogram (Fig. 9c), showing that it was even polar than the most polar major metabolite, M3. This product had a mass difference of C_3H_4O than the drug (Table 5). The absence of typical neutral losses of 42 and 92 Da, absence of fragment of *m*/*z* 375 (Table 6), and the presence of characteristic fragment of *m*/*z* 680 (Table 7) confirmed that it was a desacetylated product, similar to M3. The mass formula difference of CH_2, i.e., $C_3H_4O - C_2H_2O$ (Table 5) and the presence of intense peaks of *m*/*z* 385 and 505, similar to demethylated metabolite M10 (Figs. 10 and 12), also showed that this metabolite was further demethylated. The absence of peaks of *m*/*z* 399 and 519 indicated that demethylation occurred at piperazine moiety in part D of the drug (Fig. 1), similar to M10. This metabolite was not observed in the *in vitro* systems. Also, it was present in minor amounts in feaces, and in trace amounts in urine and plasma.

As shown in Table 5, eight metabolites, M4, M6–M8, M12, M15, M16 and M19, had the same mass of *m*/*z* 839, though their chromatographic retention was different (Fig. 9e). This indicated that all of them were isobaric. Accurate mass analyses showed addition of an oxygen atom (15.9949 Da, Table 5), denoting a single step metabolic change. Among them, M12 was easily identified as rifampicin *N*-oxide through RR_T matching, and similarity of the fragmentation pattern with the standard. In rest of the cases, it was assumed that oxidation occurred at other possible sites in the drug molecule. To delineate the same, fragmentation pattern of each, as given in Table 6, was studied critically. Unfortunately, a reasonable fragmentation profile was obtained only for metabolites M4 and M6–M8, and not for the others. In case of metabolites M4 and M7, M8, the presence of fragment of *m*/*z* 399, which was also present in the drug (Table 6), meant that parts C and D (Fig. 1) were unchanged. The presence of fragments of *m*/*z* 373, 331 and 313 (Table 6 and Fig. 12) indicated that the change happened either at part A or B (Fig. 1). Support for part A was provided again by the reported study on rifabutin [32], where oxidation was shown

to happen at similar site, as in rifampicin. There was an opposite behaviour in case of metabolite M6, wherein appearance of mass peaks of *m*/*z* 375 and 333 clearly indicated that parts A and B of rifampicin molecule (Fig. 1) were intact. The change rather happened at the aromatic side or piperazine moiety (parts C or D in Fig. 1). The same was further supported by the presence of fragments of *m*/*z* 415 and 397 (Fig. 12). Among the two parts, site of oxygenation was postulated to part D (Fig. 1), as the change was less possible at part C due to the steric hindrance, more specifically, the *N*-methyl group, due to higher polarity of M6 than metabolites M15, M16 and M19 (Table 5). The metabolites M15, M16 and M19 eluted very closely and in all the three cases, their fragmentation pattern was not complete. So, just based on their polarity behaviour with respect to other metabolites and depending upon the literature reports on *N*-oxides [35–38], these were assumed to be *N*-oxide products at remaining nitrogen atoms in part D of the drug (Fig. 1). All the mono-oxygenation products were seen in the *in vitro* RLM and HLM, and *in vivo* feaces samples. M8 was present in highest concentration, followed by M12 and non-polar mono-oxygenated metabolites (Table 8). The proposed sites of oxidation and their MS fragmentation patterns are shown in Fig. 12.

An interesting case was that of minor metabolite M9, which showed the same fragmentation pattern and accurate mass data, as the drug (Tables 5–7 and Fig. 11). It was proposed to be an acetyl derivative of the major drug metabolite, desacetylrifampicin (M3), but involving 21C/23C position instead of 25C (Fig. 1). The metabolite was present in all the *in vitro* and *in vivo* matrices. Another minor metabolite, M11, was isobaric (*m*/*z* 809) to M10 (*N*-demethylrifampicin), but had a different fragmentation profile (Table 6 and Fig. 12). In this case, typical peaks of *m*/*z* 399 and 519, and the absence of characteristic loss of 32 Da (CH_3OH) helped to propose that it was an *O*-demethylation product (Fig. 12). M11 was only observed in HLM, RLM and feaces. The metabolite M13 (*m*/*z* 684) was established to be desacetyl-3-formylrifamycin, based on the fragmentation profile and comparison of the same with M3 and M17 (Tables 6 and 7 and Fig. 10). The presence of fragments of *m*/*z* 616, 598 and 302 confirmed it to be a derivative of 3-formylrifamycin (M17). Further desacetylation in the second generation step was confirmed by the absence of neutral losses of 42 and 92 Da. The metabolite did not appear in the *in vitro* systems, indicating role of non-hepatic enzyme systems during its formation *in vivo*, where also it was formed only in minor or trace quantities. That was justified because the precursor of M13, *i.e.*, 3-formylrifamycin (M13) itself was absorbed only in small quantities due to very low solubility in gastric tract as discussed earlier. Whatever small quantities reached the liver were desacetylated, generating M13 in the process.

The last two minor metabolites, M18 and M21, had the same *m*/*z* value of 837, but appeared at different RR_T values of 1.29 and 1.44 (Table 5). The mass of both was 2 Da less than mono-oxygenated metabolites, or 16 Da more than rifampicin quinone (M20). This meant formation of either quinone derivatives of mono-oxygenated metabolites, or addition of oxygen to rifampicin quinone. Exact structure elucidation could not be done for the two, just based on the mass fragmentation studies (Fig. 13). The two metabolites were observed in all the *in vitro* conditions, and in feaces, while M21 was also found in plasma.

4. Conclusion

The present study, involving *in silico* tools, an optimized sample preparation approach and modern LC–MS techniques, showed formation of several new metabolites of rifampicin than known in the literature till date. Apart from the six known metabolites (desacetylrifampicin (M3), rifampicin glucuronide (M5), *N*-demethylrifampicin (M10), 3-formylrifamycin (M17), rifampicin quinone (M20) and desacetyl-3-formylrifampicin (M13)), fifteen more were detected in the study. It was observed that while the previously reported metabolites were essentially all detected in moderate to major amounts, most of the newly detected metabolites were present in minor to trace amounts, although their relative amounts varied in the different *in vitro* and *in vivo* samples. The new metabolites were of eight types, *viz.*, mono-oxygenated-desacetyl (M1 and M14), demethyl-desacetyl (M2), mono-oxygenated (M4, M6–M8, M12, M15, M16 and M19), acetylated-desacetyl (M9), *O*-demethyl (M11) and mono-oxygenated quinone (M18 and 21) derivatives of rifampicin. It was found that the majority of the metabolites were detected in feaces indicating that most likely this was the prominent route of excretion of rifampicin metabolites. In addition, it was observed that based on their relative amounts as compared to desacetylrifampicin, the *N*-demethylrifampicin metabolite was present as major product in faeces, while rifampicin *N*-oxide was found in almost all the matrices up to a moderate amount. Nevertheless, without the radiolabeled study or quantitative data, these are only semi-quantitative estimates of their actual amounts in the various biological samples. The identification of relatively non-polar metabolites of the drug highlights the possibility of their accumulation in body, particularly in liver, which may be responsible for the drug's hepatotoxicity. Additionally, the enzyme induction potential, which is an adverse attribute of rifampicin [20,21], may also be associated with its metabolism, particularly if non-polar metabolites were retained in the liver for a longer period. The newly identified phase I metabolites have a scope to be assessed for their efficacy, considering that desacetyl derivatives of rifampicin, rifapentine and rifabutin have activity against the mycobacteria [39,40].

Acknowledgement

The support provided by M/s Thermo Fischer Scientific (Mumbai, India) in carrying out MS^n studies is gratefully acknowledged.

References

[1] D.R. Kassel, Curr. Opin. Chem. Biol. 8 (2004) 339–345.
[2] J.M. Castro-Perez, Drug Discov. Today 12 (2007) 249–256.
[3] M.J. Gomez-Lechon, M.T. Donato, J.V. Castell, R. Jover, Curr. Drug Metab. 5 (2004) 443–462.
[4] S.S. Singh, Curr. Drug Metab. 7 (2006) 165–182.
[5] B. Suchanova, R. Kostiainen, R.A. Ketola, Eur. J. Pharm. Sci. 33 (2008) 91–99.
[6] C. Arbus, A. Benyamina, P.M. Llorca, F. Bayle, N. Bromet, F. Massiere, R.P. Garay, A. Hameg, Eur. J. Pharm. Sci. 32 (2007) 357–366.
[7] R.P. Shah, V. Kumar, S. Singh, Rapid Commun. Mass Spectrom. 22 (2008), 613-322.
[8] N. Ohashi, S. Furuuchi, M. Yoshikawa, J. Pharm. Biomed. Anal. 18 (1998) 325–334.
[9] D.J. Foltz, J. Castro-Perez, P. Riley, J.R. Entwisle, T.R. Baker, J. Chromatogr. B Analyt. Technol. Biomed. Life Sci. 825 (2005) 144–151.
[10] C. Sun, H. Xu, Y. Pan, Z. Shen, D. Wang, Rapid Commun. Mass Spectrom. 21 (2007) 2889–2894.
[11] D.Q. Liu, C.E. Hop, J. Pharm. Biomed. Anal. 37 (2005) 1–18.
[12] H. Nakagawa, Kekkaku 62 (1987) 527–547.
[13] K. Winsel, H. Iwainsky, E. Werner, H. Eule, Pharmazie 31 (1976) 95–99.
[14] S. Sunahara, H. Nakagawa, Chest 61 (1972) 526–532.
[15] G. Acocella, Clin. Pharmacokinet. 3 (1978) 108–127.
[16] C. Advenier, C. Gobert, G. Houin, D. Bidet, S. Richelet, J.P. Tillement, Ther. Drug Monit. 5 (1983) 61–65.
[17] A. Weber, K.E. Opheim, A.L. Smith, K. Wong, Rev. Infect. Dis. 5 (1983) S433–S439.
[18] A.D. Jernigan, G.D. St Jean, D.M. Rings, R.A. Sams, Am. J. Vet. Res. 52 (1991) 1626–1629.
[19] W.W. Yew, C.C. Leung, Respirology 11 (2006) 699–707.
[20] A. Tostmann, M.J. Boeree, R.E. Aarnoutse, W.C. deLange, A.J. van der Ven, R. Dekhuijzen, J. Gastroenterol. Hepatol. 23 (2008) 192–202.
[21] D.J. Pepper, G.A. Meintjes, H. McIlleron, R.J. Wilkinson, Drug Discov. Today 12 (2007) 980–989.
[22] A. Eseousse, G. Rifle, C. Sgro, C. Mousson, G. Zanetta, D. Chevet, Eur. J. Clin. Pharmacol. 48 (1995) 309–310.
[23] P. Zimniak, Ageing Res. Rev. 7 (2008) 281–300.

[24] X. Bi, Z. Meng, H. Chen, X. Zhu, G. Dou, J. Pharm. Biomed. Anal. 48 (2008) 134–139.
[25] O.H. Lowry, N.J. Rosebrough, A.L. Farr, R.J. Randall, J. Biol. Chem. 193 (1951) 265–275.
[26] M.S. Chang, Q. Ji, J. Zhang, T.A. El-Shourbagy, Drug Dev. Res. 68 (2007) 107–133.
[27] D.Q. Liu, L. Wu, M. Sun, P.A. MacGregor, J. Pharm. Biomed. Anal. 44 (2007) 320–329.
[28] P.J. Swart, F.G. Jansman, B.F. Drenth, R.A. de Zeeuw, D. Dijkstra, A.S. Horn, Pharmacol. Toxicol. 68 (1991) 215–219.
[29] C.J. Shishoo, S.A. Shah, I.S. Rathod, S.S. Savale, J.S. Kotecha, P.B. Shah, Int. J. Pharm. 190 (1999) 109–123.
[30] S. Singh, T.T. Mariappan, R. Shankar, N. Sarda, B. Singh, Int. J. Pharm. 228 (2001) 5–17.
[31] J. Li, M. Zhu, S. Rajamani, V.N. Uversky, A.L. Fink, Chem. Biol. 11 (2004) 1513–1521.
[32] I. Utkin, T. Koudriakova, T. Thompson, C. Cottrell, E. Iatsimirskaia, J. Barry, P. Vouros, N. Gerber, Drug Metab. Dispos. 25 (1997) 963–969.
[33] C. Prakash, J. O'Donnell, S.C. Khojasteh-Bakht, Drug Metab. Dispos. 35 (2007), 1071-1052.
[34] A. Deroussent, M. Re, H. Hoellinger, E. Vanquelef, O. Duval, M. Sonnier, T. Crestiel, Rapid Commun. Mass Spectrom. 18 (2004) 474–482.
[35] J. Gjerde, E.R. Kisanga, M. Hauglid, P.I. Holm, G. Mellgren, E.A. Lien, J. Chromatogr. A 1082 (2005) 6–14.
[36] S. Giri, K.W. Krausz, J.R. Idle, F.J. Gonzalez, Biochem. Pharmacol. 73 (2007) 561–573.
[37] H. Chen, Y. Chen, P. Du, F. Han, J. Pharm. Biomed. Anal. 44 (2007) 773–778.
[38] K.H. Yoon, S.Y. Lee, M. Jang, S.H. Ko, W. Kim, J.S. Park, I. Park, H.J. Kim, Talanta 66 (2005) 831–836.
[39] W.J. Burman, K. Gallicano, C. Peloquin, Clin. Pharmacokinet. 40 (2001) 327–341.
[40] N. Rastogi, K.S. Goh, M. Berchel, A. Bryskier, J. Antimicrob. Chemother. 46 (2000) 565–570.